Boundary-Layer Meteorology (2006) 119: 449–472
DOI 10.1007/s10546-005-9041-5

TANGLING TURBULENCE AND SEMI-ORGANIZED STRUCTURES IN CONVECTIVE BOUNDARY LAYERS

T. ELPERIN[1,*], N. KLEEORIN[1], I. ROGACHEVSKII[1]
and S. S. ZILITINKEVICH[2,3]

[1]*The Pearlstone Centre for Aeronautical Engineering Studies, Department of Mechanical Engineering, The Ben-Gurion University of the Negev, POB 653, Beer-Sheva 84105, Israel;*
[2]*Division of Atmospheric Sciences, Department of Physical Sciences, University of Helsinki and Finnish Meteorological Institute, Vuorikatu 15A, P.O. Box 503, 00101 Helsinki, Finland;*
[3]*Nansen Environmental and Remote Sensing Centre/Bjerknes Centre for Climate Research, NO-5059 Bergen, Norway*

(Received in final form 3 November 2005 / Published online: 14 February 2006)

Abstract. A new mean-field theory of turbulent convection is developed based on the idea that only the small-scale region of the spectrum is considered as turbulence, whereas its large-scale part, including both regular and semi-organized motions, is treated as the mean flow. In the shear-free regime, this theory predicts the convective wind instability, which causes the formation of large-scale semi-organized motions in the form of cells. In the presence of wind shear, the theory predicts another type of instability, which causes the formation of large-scale semi-organized structures in the form of rolls and the generation of convective-shear waves propagating perpendicular to the convective rolls. The spatial characteristics of these structures, such as the minimum size of the growing perturbations and the size of perturbations with the maximum growth rate, are determined. This theory might be useful for understanding the origin of large-scale cells and rolls observed in the convective boundary layer and laboratory turbulent convection.

Keywords: Convective boundary layer, Semi-organized structures, Turbulent convection.

1. Introduction

In this paper a theoretical approach proposed by Elperin et al. (2002) is further developed and applied to investigate the mechanisms of the formation of semi-organized (coherent) structures in the atmospheric convective boundary layer.

In the traditional approach, semi-organized structures are usually considered as simply the largest scale turbulent eddies. Accordingly they are treated in terms of statistical moments and corresponding turbulence

*E-mail: elperin@bgu.ac.il

closures. The term "mean flow" is applied only to the fully regular motion. In particular, shear-free convection is associated with zero mean flow, and sheared convection with the one-dimensional, plain-parallel sheared mean flow.

However, semi-organized structures that are usually observed in the atmospheric convective boundary layer (CBL) and in laboratory experiments essentially differ from turbulence. First of all, they exist and retain their specific forms during longer periods than the largest time scales of turbulence (see, e.g., Etling and Brown, 1993; Atkinson and Wu Zhang, 1996; Brümmer, 1999; and references therein). In atmospheric shear-free convection, the structures represent large, three-dimensional, long-lived Benard-type cells composed of narrow uprising plumes and wide downdraughts. They usually embrace the entire CBL (of the order of 1–3 km in height) and include pronounced convergence flow patterns close to the surface. In sheared convective flows, the structures represent CBL-scale rolls stretched along the mean wind. Buoyancy-driven structures, such as plumes, jets, and large-scale circulation patterns have been observed in numerous laboratory experiments, and the circulation caused by convection in a closed box with a heated bottom (in the Rayleigh–Benard apparatus) is often called the "convective wind" (Krishnamurti and Howard, 1981; Zocchi et al., 1990; Kadanoff, 2001; Niemela et al., 2001, and references therein). In the present study this term is used in a wider sense – to emphasize the fact that the structures do not belong to turbulence and are treated individually rather than statistically.

The lifetimes and spatial scales of semi-organized structures are larger when compared to the largest turbulent time scales. Their spectral properties differ from those of small-scale turbulence, and they are characterised by narrow spectra and do not exhibit the direct energy-cascade behaviour (from larger to smaller scales). As a result the turbulence and the structures interact in practically the same way as the turbulence and the mean flow. In other words, the structures show more similarity in their behaviour with regular flows than with turbulence. They can be identified as flows whose spatial and temporal scales are larger than the characteristic turbulent scales, whereas their time scales are shorter than the lifetime of the imposed mean flows (such as the background mean wind).

In view of the above considerations it seems natural to treat the structures in convective flows as complex but basically regular mean flows, "convective winds", and to investigate them individually rather than statistically. This is the first key point of the approach proposed by Elperin et al. (2002), which distinguishes between the "true turbulence", that is the small-scale part of the spectrum, and the "convective wind" considered together with the fully regular imposed sheared flow.

The second key point is that the true turbulence is divided into two principally different parts: the familiar "Kolmogorov-cascade turbulence" and an essentially anisotropic "tangling turbulence" caused by tangling of the mean-velocity gradients with the Kolmogorov-type turbulence (Lumley, 1967). These two types of turbulent motions overlap in the maximum-scale part of the turbulent spectrum. To parameterise the tangling turbulence, a spectral closure model is developed.

Recall that traditional theoretical models of boundary-layer turbulence, such as the Kolmogorov-type local closures, imply the following assumptions:

- fluid flows are decomposed into two components of principally different nature: organized mean flow and turbulent flow;
- turbulent fluxes are proportional to the local mean gradients, whereas the proportionality coefficients (eddy viscosity, turbulent conductivity, turbulent diffusivity) are uniquely determined by local turbulent parameters.

For example, a widely used traditional approximation of the turbulent flux of potential temperature reads

$$\mathbf{F} \equiv \langle \theta \mathbf{u} \rangle = -K_H \nabla \overline{\Theta}, \quad K_H = (1/3)\, t_{\mathrm{T}} \left\langle \mathbf{u}^2 \right\rangle,$$

where K_H is the turbulent thermal conductivity, $\overline{\Theta}$ is the mean potential temperature, t_{T} is the correlation time of the turbulent velocity field, $\mathbf{u}$ and θ are turbulent fluctuations of the velocity and potential temperature (e.g., Monin and Yaglom, 1975; Stull, 1988; Wyngaard, 1992; Garratt, 1992).

The above relation for $\mathbf{F}$ does not include the contribution from the anisotropic tangling turbulence. In fact the mean velocity gradients can directly affect the potential temperature flux. The reason is that additional essentially anisotropic velocity fluctuations are generated by tangling of the mean-velocity gradients with the Kolmogorov-type turbulence due to the influence of the inertial forces during the lifetime of large turbulent eddies. Thus the Kolmogorov turbulence feeds the energy of the tangling turbulence. In its turn the tangling turbulence causes formation of semi-organized structures due to an excitation of a large-scale instability. Anisotropic velocity fluctuations due to the tangling turbulence were studied for the first time by Lumley (1967). He had shown that the velocity field in the presence of mean shear is strongly anisotropic and is characterised by a steeper spectrum ($\propto k^{-7/3}$) than the Kolmogorov turbulence.

A turbulence closure for the tangling turbulence is formulated in $\mathbf{k}$-space (in the spectral form). As a result, there is no need for closure hypotheses for the statistical moments representing the whole spectrum of motions in physical space (the latter is an extremely difficult problem especially in

convective flows; see Zeman and Lumley, 1976; Canuto 1994; Zilitinkevich et al., 1999). The derivation of the tangling-turbulence closure model is given below (in general terms it was proposed by Elperin et al. (2002)). It includes the following steps: applying the spectral closure, solving the equations for the second moments in **k**-space, and returning to the physical space to obtain formulae for the Reynolds stresses and the turbulent heat fluxes (recall that the semi-organized structures are not included in turbulence). Besides other advantages, this procedure removes the necessity for closure hypotheses for the correlations involving pressure (the most vulnerable step in any turbulence closure). The reason is that in **k**-space, the pressure term is excluded by calculating the curl of the momentum equation.

The above tangling-turbulence closure requires us to specify a limited number of parameters, first of all the kinetic energy and the correlation length of the turbulent velocity field, characterising the background Kolmogorov turbulence. These parameters are to be calculated using comparatively simple closure models of the traditional type. Therefore, the present study – in its turbulence-closure aspect – is a complementary rather than an alternative development to the traditional turbulence closures.

Semi-organized structures in convective turbulent flows were comprehensively studied theoretically, numerically (see, e.g., Lenschow and Stephens, 1980; Wyngaard, 1983, 1987; Hunt, 1984; Moeng and Wyngaard, 1984, 1989; Mason, 1985; Shirer, 1986; Stensrud and Shirer, 1988; Hunt et al., 1988; Schmidt and Schumann, 1989; Sykes and Henn, 1989; Mahrt, 1991; Robinson, 1991; Zilitinkevich, 1991; Williams and Hacker, 1992, 1993; Chlond, 1992; Zilitinkevich et al., 1998; Young et al., 2002, and references therein), and in atmospheric experiments (Miura, 1986; Etling and Brown, 1993; Alpers and Brümmer, 1994; Atkinson and Wu Zhang, 1996; Brooks and Rogers, 1997; Brümmer, 1999; Weckwerth et al., 1999, and references therein). However, some aspects related to the origin of large-scale semi-organized structures in convective flows are not completely understood. In the atmospheric CBL and in laboratory flows, the Rayleigh numbers based on the molecular transport coefficients are very large (of the order of $10^{11} - 10^{13}$), and correspond to the fully developed turbulent convection. The effective Rayleigh numbers based on the turbulent viscosity and conductivity/diffusivity are not high. Typically they are less than the critical values required for the excitation of large-scale convection. Therefore, the emergence of large-scale convective motions in the atmospheric CBL and in laboratory flows is not completely clear.

In the present study, a new approach outlined above is applied to investigate the key excitation mechanisms of large-scale convective circulations. It is found that the convective wind instability in shear-free turbulent convection results in the formation of large-scale motions in the form of cells. In sheared convection, the instability causes the generation

of convective-shear waves. The dominant semi-organized structures in this case are rolls. The spatial characteristics of all these structures, such as the minimum size of the growing perturbations and the size of the perturbations with the maximum growth rate, are determined. A diagram of interactions between turbulent and mean-flow objects that cause the large-scale instability and formation of semi-organized structures is shown in Figure 1.

The proposed theory predicts values of the following parameters: (i) the aspect ratio L_z/L_h of the structures, where L_z and L_h are the vertical and horizontal scales of the structures; (ii) the ratios L/l_0 and T/t_T, where L is the minimum size of the semi-organized structures, l_0 is the maximum scale of turbulent motions, T is the characteristic time of formation of semi-organized structures, and t_T is the correlation time of the turbulent velocity field at the scale l_0. The theory also predicts the generation of convective-shear waves propagating perpendicular to the convective rolls whereby the flow inside the rolls is characterised by non-zero hydrodynamic helicity.

It is shown that the typical length and time scales of the convective-wind motions are larger than the true-turbulence scales. On these grounds we propose that the term turbulence (or true turbulence) will be used only for the Kolmogorov- and tangling-turbulence part of the spectrum.

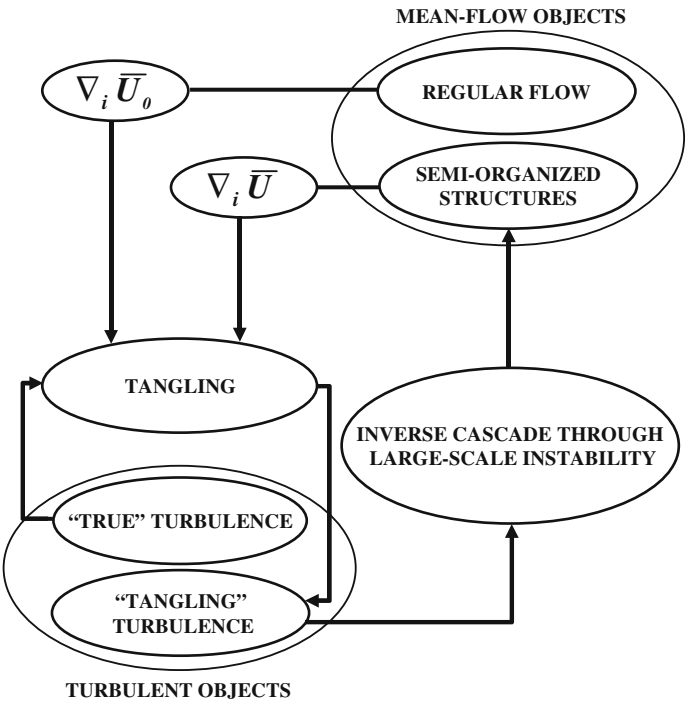

Figure 1. A scheme of interactions between turbulent and mean-flow objects causing large-scale instabilities.

This concept implies that the convective wind (as well as semi-organized motions in other very high Reynolds number flows) should not be confused with the true turbulence.

Here we need to emphasize a difference in terminology. When we refer to "Kolmogorov turbulence" we imply that starting from some scales the turbulent motions exhibit a universal behaviour. This definition coincides with Kolmogorov's understanding of fully developed turbulence. On the other hand, in the current literature on atmospheric turbulence all motions except for the mean wind are sometimes considered as turbulence.

According to atmospheric measurements in the convective boundary layer (see e.g., Kaimal et al., 1976; Kaimal and Fennigan, 1994) "the measured spectra of velocity components in the boundary layer can be generalised within the framework of mixed layer similarity. The spectrum of vertical velocity fluctuations can be reduced to a family of curves that spreads out as a function of z/z_i at low frequencies, but converge to a single universal curve in the inertial subrange. The spectra of horizontal velocity fluctuations generalised in the same manner show universal behaviour. The onset of the inertial subrange in the mixed layer occurs at wavelength $\lambda \approx 0.1 z_i$." Here z_i is the height of the lowest inversion base (typically $z_i \approx 1.25\,\mathrm{km}$). In particular, according to Kaimal et al. (1976), the universal behaviour is observed from very small scales up to $\lambda_z \approx 0.02\, z_i$ for vertical velocity fluctuations, and up to $\lambda_{x,y} \approx 0.05\, z_i$ for horizontal velocity fluctuations. In this study we refer to the Kolmogorov turbulence as turbulence with universal behaviour.

2. Tangling-Turbulence Closure Model

Since the semi-organized structures are not included in turbulence let us decompose the velocity, pressure and potential temperature fields into the "mean" component (including the semi-organized structures) and the fluctuating component characterised by zero mean values. The source of turbulence is the small-scale buoyant production. The equations for the fluctuations of velocity $\mathbf{u}$ and potential temperature θ (obtained by subtracting the equations for the "mean" fields from the corresponding equations for the total fields) read

$$\frac{\partial \mathbf{u}}{\partial t} = -\left(\overline{\mathbf{U}} \cdot \nabla\right) \mathbf{u} - (\mathbf{u} \cdot \nabla)\, \overline{\mathbf{U}} - \nabla \left(\frac{p}{\rho_0}\right) - \boldsymbol{\beta}\theta + \mathbf{U}_N, \tag{1}$$

$$\frac{\partial \theta}{\partial t} = -\left(\overline{\mathbf{U}} \cdot \nabla\right) \theta - \frac{1}{\beta} (\mathbf{u} \cdot \mathbf{e})\, N^2 + \Theta_N. \tag{2}$$

Here $\mathrm{div}\, \mathbf{u} = 0$, $\mathrm{div}\, \overline{\mathbf{U}} = 0$, $\overline{\mathbf{U}}$ is the mean velocity, $\mathbf{U}_N$ and Θ_N are the nonlinear terms that include the molecular dissipative terms, $\boldsymbol{\beta} = \mathbf{g}/T_0$ is the

buoyancy parameter (with the absolute value β), **e** is the vertical unit vector, p is the fluctuation of fluid pressure, N is the Brunt–Väisälä frequency, **g** is the acceleration of gravity (directed opposite to the vertical axis z), and T_0 and ρ_0 are the fluid temperature and density, respectively.

2.1. Derivation of the turbulent flux of potential temperature

Using Equations (1) and (2) the equations for the second moments in **k**-space, $M^{(II)}(\mathbf{k})$, can be derived:

$$\tau_{ij} = \hat{L}(u_i,\ u_j),\ F_i = \hat{L}(\theta,\ u_i),\ Q = \hat{L}(\theta,\ \omega_z),$$
$$G = \hat{L}(\omega_z,\ \omega_z),\ H = \hat{L}(\theta, \theta), \tag{3}$$

where $\boldsymbol{\omega} = \nabla \times \mathbf{u}$ are the fluctuations of vorticity and **k** is the wave vector in turbulence scales. The operator $\hat{L}$ is defined as $\hat{L}(a, b) = \langle a(\mathbf{k})\, b(-\mathbf{k})\rangle$, where the angle brackets denote ensemble averaging.

The second-moment equations include the first-order spatial differential operators $\hat{D}$ applied to the third moments $M^{(III)}$. A problem arises on how to close the system of the second-moment equations; that is how to express the set of third-order terms $\hat{D}M^{(III)}(\mathbf{k})$ through the lower moments (see Orszag, 1970; Monin and Yaglom, 1975; McComb, 1990). Various approximate methods have been proposed in order to solve this.

A widely used τ-approximation (Orszag, 1970; Pouquet et al., 1976) postulates that the deviations of the third-moment terms, $\hat{D}M^{(III)}(\mathbf{k})$, from the contributions to these terms afforded by the Kolmogorov turbulence, $\hat{D}M_K^{(III)}(\mathbf{k})$, are expressed through the similar deviations of the second moments, $M^{(II)}(\mathbf{k}) - M_K^{(II)}(\mathbf{k})$, where $M_K^{(II)}(\mathbf{k})$ is the Kolmogorov-turbulence contribution to the moment $M^{(II)}(\mathbf{k})$:

$$\hat{D}M^{(III)}(\mathbf{k}) - \hat{D}M_K^{(III)}(\mathbf{k}) = -\frac{1}{\tau_c(\mathbf{k})}\left(M^{(II)}(\mathbf{k}) - M_K^{(II)}(\mathbf{k})\right). \tag{4}$$

Here, $\tau_c(\mathbf{k})$ is the characteristic relaxation time, which can be identified with the correlation time of the turbulent velocity field, e.g., $\tau_c(\mathbf{k}) = 2t_{\mathrm{T}}(k/k_0)^{-2/3}$. The Kolmogorov-turbulence moments $M_K^{(II)}$ and $M_K^{(III)}$ are determined by the budget equations, the energy spectrum can be obtained from the dimensional analysis and the general structure of the moments is obtained by symmetry reasoning (see, e.g., Section II-C and Appendix B in Elperin et al., 2002, and references therein). It is worth noting that the above closure is consistent with the well-known $k^{-7/3}$ spectrum of the tangling turbulence.

In the present study the τ-approximation is employed to model the tangling turbulence (that is the distortion of the background turbulence caused by the spatial derivatives of the mean velocity). It is assumed that the

characteristic times of variation of the second moments are substantially larger than the correlation times $\tau_c(\mathbf{k})$ for all turbulence scales. This allows the obtaining of a stationary solution for the second moments.

To obtain the second moments through the integration over the spectrum in $\mathbf{k}$-space, Elperin et al. (2002) used a non-helical model of the background Kolmogorov-turbulence convection:

$$\tau_{ij}^{(K)}(\mathbf{k}) = \langle \mathbf{u}^2 \rangle^* P_{ij}(\mathbf{k}) \widetilde{E}(\mathbf{k}), \tag{5}$$

$$F_i^{(K)}(\mathbf{k}) = k_h^{-2} \left(k^2 F_z^{(K)}(\mathbf{k}) e_j P_{ij}(\mathbf{k}) + i Q^{(K)}(\mathbf{k}) (\mathbf{e} \times \mathbf{k})_i \right), \tag{6}$$

$$Q^{(K)}(\mathbf{k}) = -6i (k_h/k)^2 \left(\mathbf{F}^* \cdot (\mathbf{e} \times \mathbf{k}) \right) \widetilde{E}(\mathbf{k}), \tag{7}$$

$$G^{(K)}(\mathbf{k}) = \tau_{zz}^{(K)}(\mathbf{k}) k^2, \tag{8a}$$

$$H^{(K)}(\mathbf{k}) = 2H^* \widetilde{E}(\mathbf{k}), \tag{8b}$$

$$F_z^{(K)}(\mathbf{k}) = 2F_z^* \widetilde{E}(\mathbf{k}), \tag{8c}$$

where $i^2 = -1$ in Equation (7),

$$\langle \mathbf{u}^2 \rangle^* = \int \tau_{ii}^{(K)}(\mathbf{k}) \, d\mathbf{k}, \quad F_i^* = \int F_i^{(K)}(\mathbf{k}) \, d\mathbf{k}, \quad H^* = \int H^{(K)}(\mathbf{k}) \, d\mathbf{k}$$

$$\widetilde{E}(\mathbf{k}) = E(\mathbf{k})/8\pi k^2, \quad P_{ij}(\mathbf{k}) = \delta_{ij} - k_i k_j / k^2,$$

$\mathbf{k} = \mathbf{k}_z + \mathbf{k}_h$ is the wave vector comprising the vertical $\mathbf{k}_z$ and horizontal $\mathbf{k}_h$ components, $F_z^{(K)}(\mathbf{k}) = e_i F_i^{(K)}(\mathbf{k})$, $E(\mathbf{k}) = \frac{2}{3} k_0^{-1} (k/k_0)^{-5/3}$ is the Kolmogorov energy spectrum function, $k_0 = 1/l_0$ is the wavenumber, l_0 is the maximum scale of turbulent motions, the superscript (K) in Equations (5)–(8) denotes the background Kolmogorov turbulence, $F_z^* = e_i F_i^*$ is a background vertical flux of potential temperature (see more detailed discussion of this term later after Equation (10)), and $\langle \mathbf{u}^2 \rangle^*$ is the mean square velocity of the background Kolmogorov turbulence. In this study we considered a homogeneous and isotropic background turbulent convection given by Equations (5)–(8). In the previous study of Elperin et al. (2002) we showed that the effect of anisotropy of the background turbulent convection on the formation of semi-organized structures was small. Investigation of an inhomogeneous turbulent convection is a subject of separate study. Note that the correlation time t_T of turbulent velocity field satisfies the relationship

$$t_T = \frac{\int \tau_c(\mathbf{k}) E(\mathbf{k}) \, dk}{\int E(\mathbf{k}) \, dk}, \tag{9}$$

(see Monin and Yaglom, 1975).

Generally in a turbulent flow with mean velocity gradients, the total mean square velocity $\langle \mathbf{u}^2 \rangle$ is the sum of the contributions from the background Kolmogorov turbulence part, $\langle \mathbf{u}^2 \rangle^*$, and the tangling turbulence contribution. However, as is shown below (see Equation (14)), the contribution of the tangling turbulence to the total mean square velocity $\langle \mathbf{u}^2 \rangle$ is negligibly small for isotropic background Kolmogorov turbulence and an incompressible velocity field (it is determined by the higher-order spatial derivatives of the mean velocity field). Therefore, hereafter the superscript $*$ in $\langle \mathbf{u}^2 \rangle^*$ is omitted.

The model of the background turbulent convection given by Equations (5)–(8) has been derived in Appendix B of Elperin et al. (2002). This model is rather general since it is obtained using symmetry arguments under the condition of incompressibility of the flow. The key property of the Kolmogorov-type turbulence is the constant energy flux over the spectrum, which yields the equation for the correlation time of turbulent flow, $\tau_c(\mathbf{k}) = 2t_{\mathrm{T}} (k/k_0)^{-2/3}$. It is also suggested that the spectrum functions $F_z^{(K)}(\mathbf{k})$, $Q^{(K)}(\mathbf{k})$ and $H^{(K)}(\mathbf{k})$ have the same exponent of the spectrum, $q = 5/3$. Notice that the proposed tangling-turbulence theory requires only knowledge of the second moments for the background turbulent convection.

2.2. The turbulent flux of potential temperature and the Reynolds stresses

Starting from the Navier–Stokes and the potential temperature equations in the Boussinesq approximation and employing the Orszag τ-approximation, new tangling-turbulence closure equations for the total turbulent flux of potential temperature $\mathbf{F} \equiv \langle \theta \mathbf{u} \rangle$ and the Reynolds stresses $\tau_{ij} \equiv \langle u_i u_j \rangle$ are derived. The first equation reads

$$\mathbf{F} \equiv \langle \theta \mathbf{u} \rangle = \mathbf{F}^* - \frac{t_{\mathrm{T}}}{2} \left[2 \left(\nabla \cdot \overline{\mathbf{U}}_h \right) \mathbf{F}_z^* - \overline{\boldsymbol{\omega}} \times \mathbf{F}_z^* - \overline{\boldsymbol{\omega}}_{\mathbf{z}} \times \mathbf{F}^* \right]. \tag{10}$$

Here, t_{T} is the correlation time of the Kolmogorov turbulence corresponding to the maximum scale of turbulent motions, $\overline{\boldsymbol{\omega}} = \nabla \times \overline{\mathbf{U}}$ is the mean vorticity, $\overline{\mathbf{U}}$ is the mean velocity (that is the sum of the vertical $\overline{\mathbf{U}}_z$ and horizontal $\overline{\mathbf{U}}_h$ velocities: $\overline{\mathbf{U}} = \overline{\mathbf{U}}_h + \overline{\mathbf{U}}_z$), z is the vertical coordinate, and

$$F_i^* = -K_{ij} \nabla_j \overline{\Theta} - t_{\mathrm{T}} \left(\mathbf{F}^* \cdot \nabla \right) \overline{U}_i^{(eq)}(z), \tag{11}$$

is the turbulent flux of potential temperature, which is the sum of the contribution due to the Kolmogorov turbulence and a contribution of the tangling turbulence caused by shear of the imposed large-scale mean wind $\overline{U}_i^{(eq)}(z)$, and

$$K_{ij} = K_H \left[\delta_{ij} + \frac{3}{2} (2+\gamma) e_i e_j \right] \tag{12}$$

is a generalised anisotropic turbulent heat conductivity, γ is the ratio of specific heats, and K_H is the turbulent heat conductivity. The equation for the tensor K_{ij} was derived in Appendix A of Elperin et al. (2002) using the budget equations for the turbulent kinetic energy, fluctuations of the potential temperature and the heat flux. The anisotropic part of the tensor K_{ij} (the second term in the square brackets) is caused by a modification of the mean flux of potential temperature by the buoyancy effects.

The terms in the square brackets in the right-hand side of Equation (10) are caused by the tangling turbulence and depend on the "mean" (including semi-organize structures) velocity gradients. It is shown below that these terms lead to the excitation of large-scale instability and the formation of semi-organized structures. In Equation (10) the terms with zero divergence are omitted, because only $\nabla \cdot \mathbf{F}$ contributes to the mean-field dynamics. Neglecting the tangling-turbulence term and the anisotropy of turbulence this reduces to the traditional equation: $\mathbf{F} = -K_H \nabla \overline{\Theta}$.

The physical meaning of Equation (10) is elucidated as follows. The second term in Equation (10) describes the redistribution of the vertical background heat flux by convergent (or divergent) horizontal mean flows. This redistribution occurs during the lifetime of turbulent eddies (see Figure 2). The third term in Equation (10) determines the formation of the horizontal heat flux due to "rotation" of the vertical background heat flux by the horizontal mean vorticity (see Figure 3). The last term in Equation (10) describes the formation of the horizontal heat flux through the "rotation" of the horizontal background heat flux (the counterwind heat flux) by the vertical component of the mean vorticity (see Figure 4). These two effects are determined by the local inertial forces in a sheared mean flow. A more detailed discussion of Equation (10) is given in Section 3.

The above procedure also yields the Reynolds stresses:

$$\tau_{ij} \equiv \langle u_i u_j \rangle = \delta_{ij} \frac{\langle \mathbf{u}^2 \rangle}{3} - K_M \left(\nabla_i \overline{U}_j + \nabla_j \overline{U}_i \right), \tag{13}$$

$$K_M = \alpha t_{\mathrm{T}} \langle \mathbf{u}^2 \rangle, \tag{14}$$

where the coefficient $\alpha = (q+3)/30$ and q is the exponent of the energy spectrum of the background convective turbulence. For the Kolmogorov turbulence $q = 5/3$ so that $\alpha = 7/45$. The total tensor of Reynolds stresses $\langle u_i u_j \rangle$ is given by Equation (13) and includes the diagonal Kolmogorov-turbulence term $\delta_{ij} \langle \mathbf{u}^2 \rangle / 3$ and the tangling-turbulence term, $-K_M \left(\nabla_i \overline{U}_j + \nabla_j \overline{U}_i \right)$.

Since the Kolmogorov turbulence is isotropic and homogeneous, its contribution to the Reynolds stresses in the form $\delta_{ij} \langle \mathbf{u}^2 \rangle / 3$ is a natural result.

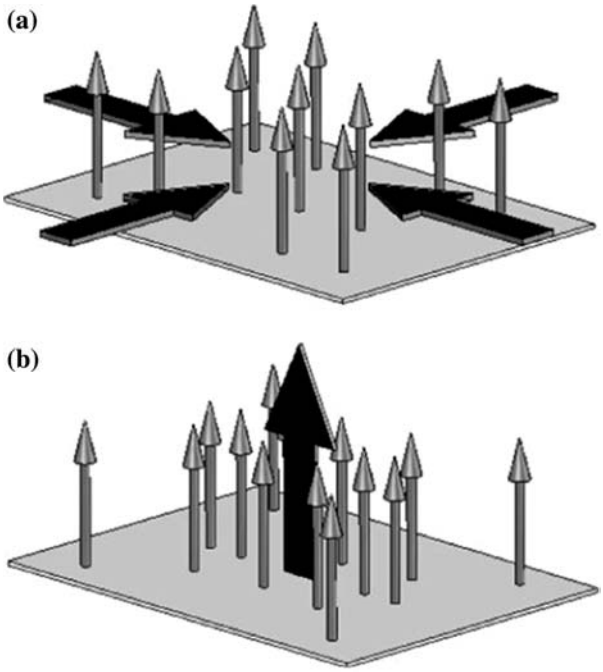

Figure 2. The effect of non-zero $\nabla \cdot \overline{\mathbf{U}}_h$, which causes redistribution of the vertical turbulent flux of potential temperature and excitation of a large-scale instability. The vertical arrows denote the vertical turbulent flux of potential temperature, and the thick horizontal arrows denote the converging horizontal flow.

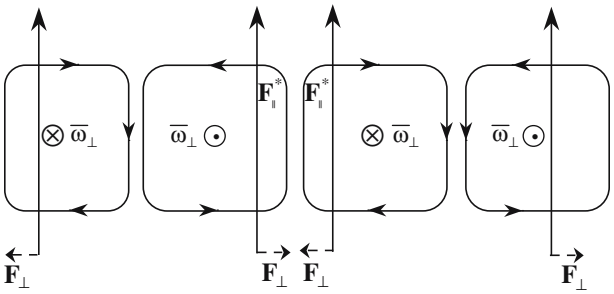

Figure 3. The effect of non-zero $\overline{\boldsymbol{\omega}} \times \mathbf{F}_z^*$, which causes horizontal potential-temperature fluxes $\mathbf{F}_y$ and decreases (increases) the "mean" potential temperature in the regions with upward (downward) flows.

The tangling-turbulence contribution to the Reynolds stresses caused by the mean velocity gradients has the traditional form, with the only difference being that the coefficient α in the expression for the turbulent viscosity K_M is calculated using the τ-approximation.

The above tangling-turbulence closure can be easily extended to parameterise the turbulent transports of passive scalars, such as suspended fine

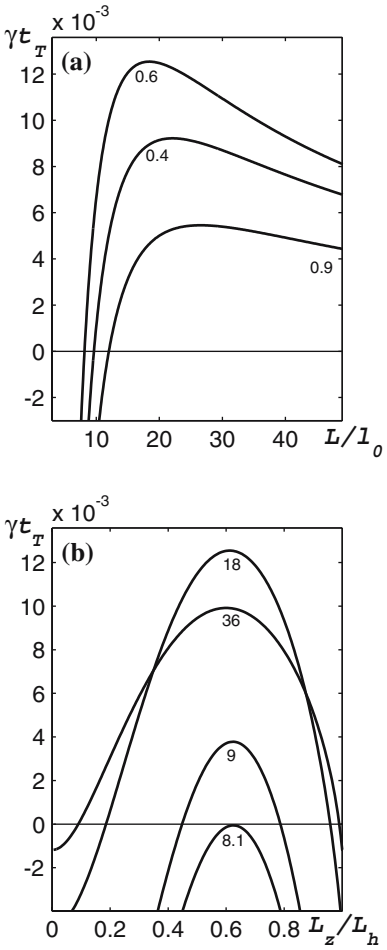

Figure 4. The growth rate of the convective-wind instability versus (a) L/l_0 (for $L_z/L_h = 0.4, 0.6, 0.9$) and (b) L_z/L_h (for $L/l_0 = 8.1, 9.0, 18, 36$).

particles or gaseous admixtures. Clearly this closure model can be used in a number of applications beyond the scope of the large-scale convective instability problem considered here in.

The Kolmogorov fine-scale turbulence and larger coherent structures can be distinguished as follows. Calculation of the two-point instantaneous correlation function $\langle u_i(t,\ \mathbf{x})u_i(t,\ \mathbf{y})\rangle$ of the turbulent velocity field yields the correlation length l of the velocity fluctuations. Calculation of the one-point two-time correlation function $\langle u_i(t_1, \mathbf{x})u_i(t_2, \mathbf{x})\rangle$ of the turbulent velocity field yields the correlation time t_{T} of the velocity fluctuations. The root-mean-square velocity u can also be determined independently from measurements. In the same way, i.e., measuring one-point two-time correlation function of the velocity field, one can determine the correlation time t_{cs} inside the

coherent structures. For the non-turbulent mode (coherent structures), the time $t_{cs} >> L/V_m$, and for the turbulent mode $t_T \approx l/u$, where L is the size of the coherent structure, and V_m is the maximum velocity inside the coherent structure. In addition, for the non-turbulent mode there is no universal spectrum and universal behaviour. The convective coherent structures are essentially heterogeneous, while the turbulence is usually close to statistical homogeneity. These features were observed in numerous laboratory experiments on turbulent convection (e.g., Niemela et al., 2001).

3. Large-Scale Instability Mechanisms and Typical Semi-Organized Structures

The formation of the semi-organized structures is described by the following mean-field equations:

$$\left(\frac{\partial}{\partial t} + \overline{\mathbf{U}} \cdot \nabla\right) \overline{U}_i = -\nabla_i \left(\frac{\overline{P}}{\rho_0}\right) - \nabla_j \tau_{ij} + \beta \overline{\Theta} e_i, \tag{15}$$

$$\left(\frac{\partial}{\partial t} + \overline{\mathbf{U}} \cdot \nabla\right) \overline{\Theta} = -\nabla \cdot \mathbf{F} - \frac{N^2}{\beta} \overline{U}_z, \tag{16}$$

where the turbulent flux of potential temperature $\mathbf{F}$ and the Reynolds stresses τ_{ij} are determined by Equations (10) and (13), $\overline{P}$ is the mean pressure, $\beta = g/T_0$ is the buoyancy parameter, and $\mathbf{e}$ is the vertical unit vector directed along the z-axis.

3.1. Linearised equations

The key point of the present study is the formation of semi-organized structures by a large-scale instability. Consider the linear stage of the large-scale instability. We linearise Equations (15)–(16) for small perturbations from the equilibrium. The equations for small perturbations $\widetilde{U}_z = \overline{U}_z - \overline{U}_z^{(eq)}$, $\widetilde{\omega}_z = \overline{\omega}_z - \overline{\omega}_z^{(eq)}$, and $\widetilde{\Theta} = \overline{\Theta} - \overline{\Theta}^{(eq)}$ are given by

$$\Delta \left(\frac{\partial}{\partial t} + \overline{\mathbf{U}}^{(eq)} \cdot \nabla\right) \widetilde{U}_z = \frac{\partial}{\partial z} \left(\nabla_i \nabla_j \tilde{\tau}_{ij}\right) - \Delta \left(e_i \nabla_j \tilde{\tau}_{ij}\right) + \beta \Delta_h \tilde{\Theta}, \tag{17}$$

$$\left(\frac{\partial}{\partial t} + \overline{\mathbf{U}}^{(eq)} \cdot \nabla\right) \tilde{\omega}_z = -\left(\mathbf{e} \times \nabla\right)_i \left[\nabla_j \tilde{\tau}_{ij} + \tilde{U}_z \frac{\partial \overline{U}_i^{(eq)}}{\partial z}\right], \tag{18}$$

$$\left(\frac{\partial}{\partial t} + \overline{\mathbf{U}}^{(eq)} \cdot \nabla\right) \tilde{\Theta} = -\nabla \cdot \widetilde{\mathbf{F}} - \frac{N^2}{\beta} \widetilde{U}_z, \tag{19}$$

$$\nabla\cdot\tilde{\mathbf{F}}=-\frac{t_{\mathrm{T}}}{2}\left[F_z^*\left(2\Delta_h-\Delta\right)\widetilde{U}_z+\left(\left(\mathbf{F}^*\times\mathbf{e}\right)\cdot\nabla\right)\tilde{\omega}_z\right]-K_{ij}\nabla_i\nabla_j\widetilde{\Theta}. \tag{20}$$

Here, the expression for $\nabla\cdot\widetilde{\mathbf{F}}$ follows from Equation (10), $\widetilde{\tau}_{ij}=-K_M\left(\nabla_i\widetilde{U}_j+\nabla_j\widetilde{U}_i\right)$ are the Reynolds stresses for perturbations of the mean velocity, K_M is the turbulent viscosity given by Equation (14), $\Delta_h=\Delta-\partial^2/\partial z^2$ is the horizontal Laplace operator. Recall that the total Reynolds stresses tensor $\langle u_i u_j\rangle=\delta_{ij}\langle\mathbf{u}^2\rangle/3+\tilde{\tau}_{ij}$, includes the diagonal Kolmogorov-turbulence term besides the tangling-turbulence term $\widetilde{\tau}_{ij}$. In this study we neglected $\nabla_i K_M$ and $\nabla_i K_H$, i.e., we neglected the heterogeneity of turbulent convection. This issue will be addressed in a separate paper.

For shear-free convection the equilibrium state (i.e., the state with zero time derivatives in Equations (15)–(16)) is given by $\overline{\mathbf{U}}^{(eq)}=\overline{\boldsymbol{\omega}}^{(eq)}=0$, while for sheared convection the equilibrium state is determined by $\overline{\mathbf{U}}^{(eq)}(z)=\left(\lambda/t_{\mathrm{T}}\right)z\mathbf{e}_y$ and $\overline{\boldsymbol{\omega}}^{(eq)}=-\left(\lambda/t_{\mathrm{T}}\right)\mathbf{e}_x$. Here λ is the dimensionless wind shear, $\mathbf{e}_x$ and $\mathbf{e}_y$ are unit vectors in the horizontal plane. Note that in the considered equilibrium states, div $\mathbf{F}^*=0$. However, this does not imply that the total turbulent flux of potential temperature in the presence of semi-organized structures is constant. The variables $\tilde{\mathbf{U}},\tilde{\boldsymbol{\omega}}$ and $\tilde{\Theta}$ describe semi-organized structures.

Considering the linear stage of large-scale instability we seek the solution of the linearised mean-field equations (17)–(20) in the form $\propto\exp\left(i\mathbf{k}\cdot\mathbf{R}-\gamma_{\mathrm{inst}}t\right)$, which allows us to determine the growth rate of the instability. In this analysis we assume that the heterogeneity of the turbulence is weak, i.e., we neglected $\nabla_i K_M$ and $\nabla_i K_H$. Our recent numerical simulations demonstrated that accounting for the vertical heterogeneity of the turbulence, and using different types of boundary conditions, change the final results insignificantly.

3.2. Shear-free convection

In the shear-free regime, the convective-wind instability is related to the first term in square brackets in Equation (10) for the turbulent flux of potential temperature. When $\partial\overline{U}_z/\partial z>0$, perturbations of the vertical velocity $\overline{U}_z$ cause negative divergence of the horizontal velocity, $\nabla\cdot\overline{\mathbf{U}}_h<0$ (provided that $\nabla\cdot\overline{\mathbf{U}}\approx 0$). This strengthens the local vertical turbulent flux of potential temperature and by this means leads to increasing of the local "mean" potential temperature and buoyancy (see Figure 2). The latter enhances the local "mean" vertical velocity $\overline{U}_z$. Through this mechanism a large-scale instability is excited. Similar reasoning is valid when $\partial\overline{U}_z/\partial z<0$, whereas $\nabla\cdot\overline{\mathbf{U}}_h>0$. In this case a negative perturbation of the vertical flux of potential temperature leads to a decrease of the "mean" potential temperature and buoyancy, which enhances the downward flow, and once

again excites the instability. Thus, a non-zero $\nabla \cdot \overline{\mathbf{U}}_h$ causes redistribution of the vertical turbulent flux of potential temperature and the formation of regions with large values of this flux. The regions where $\nabla \cdot \overline{\mathbf{U}}_h < 0$ alternate with the low-flux regions where $\nabla \cdot \overline{\mathbf{U}}_h > 0$. This mechanism causes the formation of large-scale flow patterns (semi-organized structures).

The role of the second term in square brackets in Equation (10) is to decrease the growth rate of the convective-wind instability. Indeed, the interaction of the "mean" vorticity with the vertical flux of potential temperature produces the horizontal heat flux (see Figure 3). The latter decreases (increases) the "mean" potential temperature in the regions with upward (downward) local flows, thus relaxing the buoyancy forces and reducing the "mean" vertical velocity $\overline{U}_z$ and the "mean" vorticity $\overline{\boldsymbol{\omega}}$. This mechanism dampens the convective-wind instability.

The above two competitive effects, namely (i) redistribution of the vertical heat flux due to convergence/divergence of the horizontal "mean" flows, and (ii) production of the horizontal component of the heat flux due to the interaction of the mean vorticity with its vertical component, determine the growth rate of the convective-wind instability.

Perturbative analysis of the linearised Equations (17)–(19) in the shear-free convection regime (when $\overline{\mathbf{U}}^{(eq)} = 0$) yields the following expression for the growth rate γ_{inst} of longwave perturbations ($h \gg 1$):

$$\gamma_{\text{inst}} \propto g F_z^* t_{\text{T}}^2 k^2 \sqrt{h} \, |\sin\varphi| \sqrt{1 - 2\sin^2\varphi}. \tag{21}$$

Here, $h = 1/(l_0 k)^2$, l_0 is the maximum scale of turbulent motions, φ is the angle between the vertical unit vector $\mathbf{e}$ and the wave vector $\mathbf{k}$ of small perturbations.

In the case considered above, $N^2 << g t_{\text{T}} |\mathbf{F}^*| k_{z,h}^2$, and allowed neglecting the term $\widetilde{U}_z N^2$ in the right-hand side of Equation (19). Our recent numerical simulations accounting for this term have shown that its role in the excitation of the large-scale instability is minor compared with the effects caused by the new terms in the heat flux Equation (10). In particular, when we neglected the new terms in Equation (10) and took into account the term $\widetilde{U}_z N^2$, the critical Rayleigh number required for the excitation of the large-scale instability was very high (≈ 2500). However, taking into account the new terms in Equation (10), namely the terms associated with the modification of the vertical background heat flux by the convergent or divergent horizontal mean flows or by the mean vorticity, we have found that the threshold required for the excitation of the large-scale instability strongly decreased (by an order of magnitude).

For large $h = 1/(l_0 k)^2$ the growth rate of the instability is proportional to the wavenumber k (i.e., $\gamma_{\text{inst}} \propto k u_0$), and the instability occurs when $tg\varphi < 1$. Here, u_0 is the characteristic turbulent velocity at the maximum scale of

turbulent motions. This range for the instability corresponds to the aspect ratio $0 < L_z/L_h < 1$, where $L_z/L_h \equiv k_h/k_z = \tan\varphi$, $L_z = 2\pi/k_z$ and $L_h = 2\pi/k_h$. The growth rate of the convective-wind instability is independent of the direction of the horizontal wavenumber. Thus it is plausible to conclude that the form of the large-scale semi-organized structure should be symmetric in the horizontal plane, e.g., in the form of cells.

Figure 4 shows the growth rate of the instability as a function of the parameters L/l_0 (Figure 4a) and L_z/L_h (Figure 4b), where $L = 1/\sqrt{L_z^{-2} + L_h^{-2}}$. The maximum growth rate of instability, $\gamma_m \approx 0.045 t_{\mathrm{T}}^{-1}$, is achieved at the scale of perturbations $L_{\mathrm{m}} \approx 10 l_0$. The characteristic time of excitation of this instability is of the order of (20–30) t_{T}. The typical length and time scales of the convective-wind motions are much larger than the turbulence scales.

3.3. Sheared convection

The convective-shear instability is related to the third term in square brackets in Equation (10). The key role here is played by the generation of the potential temperature perturbations by vorticity perturbations. Indeed, in two adjacent vortices with the opposite directions of the vertical vorticity $\overline{\boldsymbol{\omega}}_{\mathbf{z}}$ ("a" and "b" in Figure 5), the turbulent fluxes of potential temperature are directed towards the boundary between the vortices. This increases the "mean" potential temperature and the buoyancy, and generates the upward flow between the vortices. Similarly, between the vortices "b" and "c" shown in Figure 5, the "mean" potential temperature and buoyancy decreases, which generates the downward "mean" flow. These vertical flows excite vorticity perturbations. Thus the instability mechanism is sustained.

Perturbation analysis of the linearised Equations (17)–(19) in the sheared convection regime yields the following relation for a growth rate of long-wave perturbations:

$$\gamma_{\mathrm{inst}} \propto g F_z^* t_{\mathrm{T}}^2 k^2 \left(h\lambda \sin^2\varphi\right)^{2/3}, \tag{22}$$

where $\lambda = t_{\mathrm{T}} \partial \overline{U}^{(eq)}/\partial z$ is the dimensionless wind shear, and $k = \sqrt{k_x^2 + k_z^2}$ is the wavenumber. The reference state is characterised by depth-constant large-scale wind shear, $\overline{\mathbf{U}}^{(eq)} = \left(\lambda/t_{\mathrm{T}}\right) z \mathbf{e}_y$.

We considered the case when $N^2 \ll g t_{\mathrm{T}} |\mathbf{F}^*| k_{z,h}^2$, which allowed neglecting the term $\tilde{U}_z N^2$ on the right-hand side of Equation (19). We also investigated the convective-shear instability for the very small component of the wavenumber along the imposed mean wind ($k_y \to 0$, which implies uniform perturbations along the wind). This case corresponds to the maximum growth rate of the convective-shear instability. When $k_y = 0$, we obtained

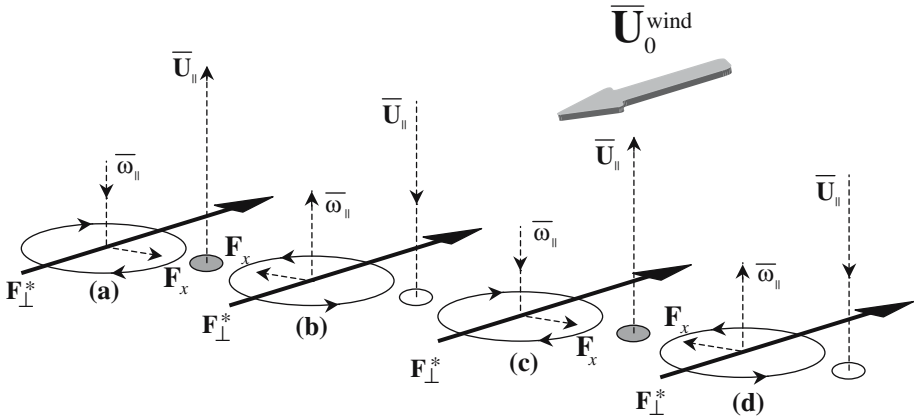

Figure 5. The effect of non-zero $\overline{\boldsymbol{\omega}}_z \times \mathbf{F}^*$, which causes redistribution of the horizontal turbulent flux of potential temperature. For two vortices ("a" and "b") with opposite directions of the vorticity $\overline{\boldsymbol{\omega}}_z$, the turbulent flux of potential temperature is directed towards the boundary between the vortices. The latter increases the mean potential temperature between the vortices "a" and "b". For the vortices "b" and "c" the situation is opposite, so that the mean potential temperature between the vortices decreases.

the algebraic dispersion relations with constant coefficients. Moreover, we considered the boundary-layer problem for $k_y \neq 0$ and found that the final results did not change strongly. This analysis allowed explanation of the observed angles between the wind and the direction of the rolls (cloud streets) when the growth rate of the instability is maximum. We also found that changing the boundary conditions did not strongly affect the final results, but only slightly changes the ranges of the instability and modifies the growth rate of the instability.

This instability causes formation of large-scale semi-organized fluid motions, e.g., in the form of rolls stretched along the imposed mean wind. This mechanism can also result in generation of the convective-shear waves with frequency Ω given by

$$\Omega \propto g F_z^* t_T^2 k^2 \left(h\lambda \sin^2 \varphi\right)^{2/3}, \tag{23}$$

which implies the wavenumber dependence: $\Omega \propto k^{2/3}$. The convective-shear waves propagate perpendicular to convective rolls. The predicted motions in convective rolls are characterised by non-zero helicity, in agreement with Etling (1985). Note that similar waves propagating in the direction normal to cloud streets have been detected in the atmospheric CBL (see Brümmer, 1999).

Figure 6 shows the range of parameters L_z/L_h and L/l_0 where convective-shear instability occurs, for different values of the wind-shear parameter λ. The increase of shear is favourable for the excitation of the

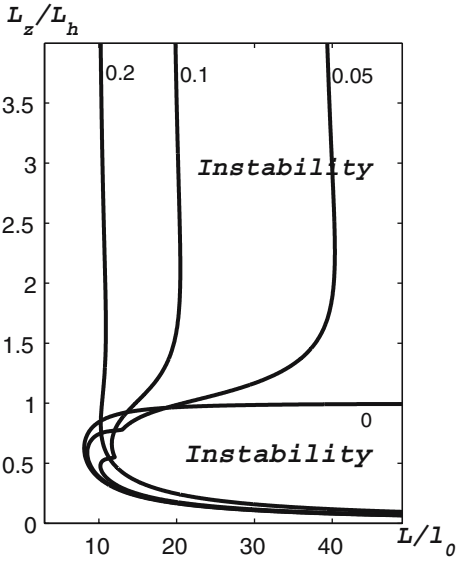

Figure 6. The range of parameters L_z/L_h and L/l_0, where the convective-shear instability occurs for different values of the dimensionless shear: $\lambda = 0, 0.05, 0.1, 0.15$. The case $\lambda = 0$ corresponds to the convective-wind instability.

convective-shear instability with the growth rate $\gamma_{\text{inst}} \propto k^{2/3}$. The case $\lambda = 0$ in Figure 6 corresponds to the convective-wind instability. Figure 7 shows the growth rates of the convective-shear instability, and Figure 8 shows the frequencies of the generated convective-shear waves.

As seen from Figure 7 the first derivative $d\gamma_{\text{inst}}/dk$ has a point of singularity at $L = L_*$, which is indicative of bifurcation. Indeed, the growth rate of the convective-shear instability is determined by a cubic algebraic equation that follows from Equations (17)–(19). When $L < L_*$, this equation has three real roots, which corresponds to aperiodic instability. When $L > L_*$, it has one real and two complex conjugate roots. Therefore, $L = L_*$ is the bifurcation point, and when $L > L_*$ the convective-shear waves are generated. Notice that L_* decreases with increasing L_z/L_h. When $L_z > L_h$, it becomes smaller than the threshold L_{cr} for the excitation of the large-scale instability. In this case the convective rolls are always accompanied by propagating convective-shear waves. Note also that for any given L/l_0, there are the lower and the upper limits for the values of L_z/L_h for which the convective-shear instability can be excited. When L/l_0 is large enough, the range of the instability has no upper limit with respect to L_z/L_h. Notably the flow in the convective-shear wave has a non-zero hydrodynamic helicity.

For perturbations with $k_x = 0$ the convective-shear instability is not excited, whereas the convective wind instability can be excited. The above

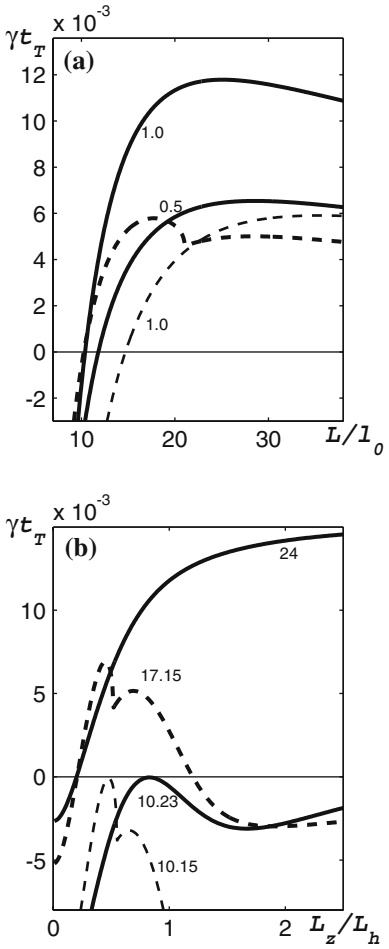

Figure 7. The growth rate of the convective-shear instability versus (a) L/l_0 ($L_z/L_h = 0.5, 1.0$) and (b) L_z/L_h ($L/l_0 = 10.15, 10.23, 17.15, 24$) for different values of the dimensionless shear: $\lambda = 0.1$ (dashed lines) and $\lambda = 0.2$ (solid lines).

large-scale instabilities are fed by the energy of the true turbulence, and so exhibit an inverse energy cascade. The main difference from the familiar inverse cascade in the two-dimensional turbulence is the pivotal role of the thermal processes, i.e., redistribution of the heat flux by large-scale "mean" flows. Our analysis shows that in two-dimensional turbulence the large-scale instability cannot be excited.

The results discussed in this section might be useful for understanding the basic features of semi-organized structures observed in the atmospheric CBL and in laboratory turbulent convection.

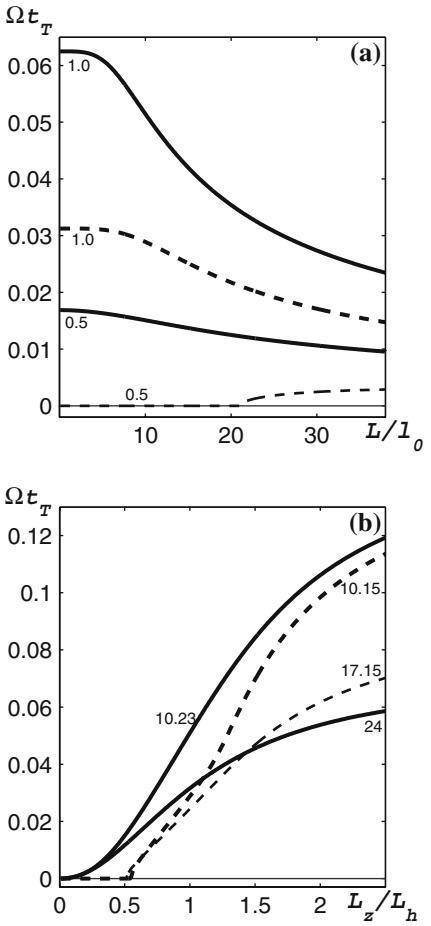

Figure 8. Frequencies of the generated convective-shear waves versus (a) L/l_0 (for $L_z/L_h = 0.5, 1.0$) and (b) L_z/L_h (for $L/l_0 = 10.15, 10.23, 17.15, 24$) for different values of the dimensionless shear: $\lambda = 0.1$ (dashed lines) and $\lambda = 0.2$ (solid lines).

4. Conclusions

The proposed approach distinguishes between the two principally different types of irregular motions. The first one is the true turbulence representing the small-scale, turbulent part of the spectrum, which is treated statistically and parameterised with the aid of an appropriate turbulence closure model. The second type represents semi-organized motions (convective wind) caused by large-scale instabilities and fed by the energy of the true turbulence through the inverse energy cascade. Typical scales of these motions are much larger than the largest true-turbulence scales. They are treated as very complex but quasi-regular "mean" flows. In the present study their key properties are determined using perturbation analysis.

The true turbulence in its turn comprises two different contributions: the familiar "Kolmogorov-cascade turbulence" and strongly non-isotropic "tangling turbulence" caused by tangling of the mean-velocity gradients with the Kolmogorov turbulence. An advanced turbulence closure model for the tangling turbulence is derived.

On the basis of the above developments it is conceivable to suggest that the term turbulence (or true turbulence) will be used only for the Kolmogorov and tangling-turbulence part of the spectrum. The convective wind (as well as semi-organized motions in other very high Reynolds number flows) should not be confused with the true turbulence. Moreover, further attempts to develop an overall turbulence closure covering the whole spectrum of non-regular motions in convective flows do not look promising. Indeed, traditional mathematical-statistical tools, though quite adequate as applied to the true turbulence, become a Procrustean bed for semi-organized motions such as the convective wind. This inconsistency explains why modern convective-turbulence closures, despite their enormous complexity, are not sufficiently advanced to reproduce the transport properties of convective flows over a range of regimes.

In accordance with the convective-wind concept, the following threefold approach is proposed, instead of the traditional (overall) closures, to model convective flows of practical importance:

- Application of (i) the traditional local closures to the Kolmogorov turbulence and (ii) the newly proposed Orszag-type (relaxation) closure to the tangling turbulence;
- analytical investigation of basic features and scales of the convective-wind structures through perturbation analyses using the above closures;
- three-dimensional numerical simulation of the flows under consideration with optimal spatial resolution imposed by the perturbation analysis, which is resolving only the dominant, rapidly growing modes, and using advanced tangling-turbulence closures to parameterise unresolved small-scale motions.

Acknowledgements

The authors benefited from stimulating discussions with F. Busse, D. Etling, H.J.S. Fernando, R. Foster, S. Grossmann, J.C.R. Hunt, A. Tsinober and V. Yakhot. We are grateful to three anonymous referees for their helpful comments. This work was partially supported by the German–Israeli Project Cooperation (DIP) administrated by the Federal Ministry of Education and Research (BMBF), the Israel Science Foundation governed by the Israeli Academy of Science, the Swedish Institute Project 2570/2002 (381/N34),

the EU Project FUNAPEX EVK4-CT-2002-00097, and the International Meteorological Institute of Stockholm University. SSZ acknowledges support from the EU Marie Curie Chair Project MEXC-CT-2003-509742, and ARO Project "Advanced parameterisation and modelling of turbulent atmospheric boundary layers" – contract number W911-NF-05-1-0055.

Appendix A: The Energetic Aspect of the Large-scale Instability

Let us discuss the energetic aspect of the linearised analytical treatment (see e.g., Asai, 1970) of the large-scale instability described in Section 3. The equation for the evolution of perturbations of total energy $\widetilde{E} = \frac{\tilde{U}^2}{2} + \frac{\beta^2}{2N^2}\widetilde{\Theta}^2$ reads

$$\frac{\partial \tilde{E}}{\partial t} + \nabla \cdot \tilde{\mathbf{\Phi}} = I - D, \tag{A1}$$

where

$$D = K_M S^2 + K_H \frac{\beta^2 \left|\nabla \widetilde{\Theta}\right|^2}{N^2} \tag{A2}$$

is the dissipation, $S^2 = (\nabla_i \widetilde{U}_j)^2$, $\widetilde{\mathbf{\Phi}}$ is the third-order flux (in perturbations), and

$$I = -\widetilde{U}_y \widetilde{U}_z \frac{\partial U_y^{eq}}{\partial z} + \frac{\beta^2 \nabla_i \widetilde{\Theta}}{N^2} \widetilde{F}_i \tag{A3}$$

is the source of energy due to the mean flow shear (the first term in Equation (A3)) and the redistribution of the heat flux by the non-uniform motions caused by the velocity perturbations (described by the second term in Equation (A3)). Here

$$\widetilde{\mathbf{F}} = -\frac{t_T}{2}\left[2\left(\nabla \cdot \widetilde{\mathbf{U}}_h\right)\mathbf{F}_z^* - \widetilde{\boldsymbol{\omega}} \times \mathbf{F}_z^* - \widetilde{\boldsymbol{\omega}}_\mathbf{z} \times \mathbf{F}^*\right] \tag{A4}$$

is the new contribution to the heat flux. In order to derive Equation (A1) we used Equations (15)–(16) for perturbations.

For small values of the Brunt–Väisälä frequency, the second term in Equation (A3) for the source I becomes more important, and may cause the large-scale instability. The energy source of the instability is the energy of turbulence.

References

Alpers, W. and Brümmer, B.: 1994, 'Atmospheric Boundary Layer Rolls Observed by the Synthetic Aperture Radar Aboard the ERS-1 Satellite', *J. Geophys. Res.* **99(C6)**, 12613–12621.

Asai, T.: 1970, 'Stability of a Plane Parallel Flow with Variable Vertical Shear and Unstable Stratification', *J. Meteorol. Soc. Japan* **48**, 129–139.

Atkinson, B. W. and Wu Zhang, J.: 1996, 'Mesoscale Shallow Convection in the Atmosphere', *Rev. Geophys.* **34**, 403–431.

Brooks, I. M. and Rogers, D. P.: 1997, 'Aircraft Observations of Boundary Layer Rolls off the Coast of California', *J. Atmos. Sci.* **54**, 1834–1849.

Brümmer, B.: 1999, 'Roll and Cell Convection in Winter-Time Arctic Cold-Air Outbreaks', *J. Atmos. Sci.* **56**, 2613–2636.

Canuto, V. M., Minotti, F., Ronchi, C., Ypma, R. M., and Zeman, O.: 1994, 'Second-Order Closure PBL Model with New Third-Order Moments: Comparison with LES', *J. Atmos. Sci.* **51**, 1605–1618.

Chlond, A.: 1992, 'Three-Dimensional Simulation of Cloud Street Development during a Cold Air Outbreak', *Boundary-Layer Meteorol.* **58**, 161–200.

Elperin, T., Kleeorin, N., Rogachevskii, I., and Zilitinkevich, S.: 2002, 'Formation of Large-Scale Semi-Organized Structures in Turbulent Convection', *Phys. Rev. E* **66**, 066305 (1–15).

Etling, D.: 1985, 'Some Aspects on Helicity in Atmospheric Flows', *Contrib. Atmos. Phys.* **58**, 88–100.

Etling, D. and Brown, R. A.: 1993, 'Roll Vortices in the Planetary Boundary Layer: A Review', *Boundary-Layer Meteorol.* **65**, 215–248.

Garratt, J. R.: 1992, *The Atmospheric Boundary Layer*, Cambridge University Press, U.K., 316 pp.

Hunt, J. C. R.: 1984, 'Turbulence Structure in Thermal Convection and Shear-Free Boundary Layers', *J. Fluid Mech.* **138**, 161–184.

Hunt, J. C. R., Kaimal, J. C., and Gaynor, J. I.: 1988, 'Eddy Structure in the Convective Boundary Layer – New Measurements and New Concepts', *Quart. J. Roy. Meteorol. Soc.* **114**, 837–858.

Kadanoff, L. P.: 2001, 'Turbulent Heat Flow: Structures and Scaling', *Phys. Today* **54**, 34–38.

Kaimal, J. C. and Fennigan, J. J.: 1994, *Atmospheric Boundary Layer Flows: Their Structure and Measurement*, Oxford University Press, Oxford, 289 pp.

Kaimal, J. C., Wyngaard, J. C., Haugen, D. A., Cote, O. R., and Izumi, Y.: 1976, 'Turbulence Structure in the Convective Boundary Layer', *J. Atmos. Sci.* **33**, 2152–2169.

Krishnamurti, R. and Howard, L. N.: 1981, 'Large-Scale Flow Generation in Turbulent Convection', *Proc. Natl. Acad. Sci. USA* **78**, 1981–1985.

Lenschow, D. H. and Stephens, P. L.: 1980, 'The Role of Thermals in the Convective Boundary Layer', *Boundary-Layer Meteorol.* **19**, 509–532.

Lumley, J. L.: 1967, 'Rational approach to Relations between Motions of Different Scales in Turbulent Flows', *Phys. Fluids* **10**, 1405–1408.

Mahrt, L.: 1991, 'Eddy Asymmetry in the Sheared Heated Boundary Layer', *J. Atmos. Sci.* **48**, 472–492.

Mason, P. J.: 1985, 'A Numerical Study of Cloud Street in the Planetary Boundary Layer', *Boundary-Layer Meteorol.* **32**, 281–304.

McComb, W. D.: 1990, *The Physics of Fluid Turbulence*, Clarendon Press, Oxford, 572 pp.

Miura, Y.: 1986, 'Aspect Ratios of Longitudinal Rolls and Convection Cells Observed during Cold Air Outbreaks', *J. Atmos. Sci.* **43**, 26–39.

Moeng, C.-H. and Wyngaard, J. C.: 1984, 'Statistics of Conservative Scalars in the Convective Boundary Layer', *J. Atmos. Sci.* **41**, 3161–3169.

Moeng, C.-H. and Wyngaard, J. C.: 1989, 'Evaluation of Turbulent Transport and Dissipation Closures in Second-Order Modelling', *J. Atmos. Sci.* **46**, 2311–2330.

Monin, A. S. and Yaglom, A. M.: 1975, *Statistical Fluid Mechanics*, MIT Press, Cambridge, Massachusetts, Vol. 2, 874 pp.

Niemela, J. J., Skrbek, L., Sreenivasan K. R., and Donnelly, R. J.: 2001, 'The Wind in Confined Thermal Convection', *J. Fluid Mech.* **449**, 169–178.

Orszag, S. A.: 1970, 'Analytical Theories of Turbulence', *J. Fluid Mech.* **41**, 363–386.

Pouquet, A., Frisch, U., and Leorat, J.: 1976, 'Strong MHD Turbulence and the Nonlinear Dynamo Effect', *J. Fluid Mech.* **77**, 321–354.

Robinson, S. K.: 1991, 'Coherent Motions in the Turbulent Boundary Layer', *Annu. Rev. Fluid Mech.* **23**, 601–640.

Schmidt, H. and Schumann U.: 1989, 'Coherent Structure in the Convective Boundary Layer Derived from Large-Eddy Simulations', *J. Fluid Mech.* **200**, 511–562.

Shirer, H. N.: 1986, 'On Cloud Street Development in Three Dimensions: Parallel and Rayleigh Instabilities', *Contrib. Atmos. Phys.* **59**, 126–149.

Stensrud, D. J. and Shirer, H. N.: 1988, 'Development of Boundary Layer Rolls from Dynamical Instabilities', *J. Atmos. Sci.* **45**, 1007–1019.

Stull, R. B.: 1988, *An Introduction to Boundary Layer Meteorol*ogy, Kluwer Academic Publishers, Dordrecht, 666 pp.

Sykes, R. I. and Henn, D. C.: 1989, 'Large-Eddy Simulation of Turbulent Sheared Convection', *J. Atmos. Sci.* **46**, 1106–1118.

Weckwerth, T. M., Horst, T. W., and Wilson, J. W.: 1999, 'An Observational Study of the Evolution of Horizontal Convective rolls', *Mon. Wea. Rev.* **127**, 2160–2179.

Williams, A. G. and Hacker, J. M.: 1992, 'The Composite Shape and Structure of Coherent Eddies in the Convective Boundary Layer', *Boundary-Layer Meteorol.* **61**, 213–245.

Williams, A. G. and Hacker, J. M.: 1993, 'Interaction between Coherent Eddies in the Lower Convective Boundary Layer', *Boundary-Layer Meteorol.* **64**, 55–74.

Wyngaard, J. C.: 1983, 'Lectures on the Planetary Boundary Layer', in D. K. Lilly and T. Gal-Chen (eds.), *Mesoscale Meteorology – Theories, Observations and Models,* Reidel, Dordrecht, pp. 603–650.

Wyngaard, J. C.: 1987, 'A Physical Mechanism for the Asymmetry in Top-Down and Bottom-Up Diffusion', *J. Atmos. Sci.* **44**, 1083–1087.

Wyngaard, J. C.: 1992, 'Atmospheric Turbulence', *Annu. Rev. Fluid Mech.* **24**, 205–233.

Young, G. S., Kristovich, D. A. R., Hjelmfelt, M. R., and Foster, R. C.: 2002, 'Rolls, Streets, Waves and More', *Bull. Amer. Meteorol. Soc.* **83**, 997–1001.

Zeman, O. and Lumley, J. L.: 1976, 'Modeling Buoyancy Driven Mixed Layers', *J. Atmos. Sci.* **33**, 1974–1988.

Zilitinkevich, S. S.: 1991, *Turbulent Penetrative Convection*, Avebury Technical, Aldershot, 179 pp.

Zilitinkevich, S. S., Grachev, A., and Hunt, J. C. R.: 1998, 'Surface Frictional Processes and Non-Local Heat/Mass Transfer in the Shear-Free Convective Boundary Layer', in E. G. Plate et al. (eds.), *Buoyant Convection in Geophysical Flows*, Kluwer Academic Publications, Dordrecht, The Netherlands, pp. 83–113.

Zilitinkevich, S. S., Gryanik, V. M., Lykossov, V. N., and Mironov, D. V.: 1999, 'Third-Order Transport and Nonlocal Turbulence Closures for Convective Boundary Layers', *J. Atmos. Sci.* **56**, 3463–3477.

Zocchi, G., Moses, E., and Libchaber, A.: 1990, 'Coherent Structures in Turbulent Convection', *Physica A* **166**, 387–407.